IET Microwaves, Antennas & Propagation

Research Article

Wide-stopband and high selectivity step impedance resonator bandpass filter using T-network and antiparallel coupled line

ISSN 1751-8725
Received on 23rd October 2018
Revised 25th April 2019
Accepted on 10th May 2019
E-First on 12th June 2019
doi: 10.1049/iet-map.2018.5947
www.ietdl.org

Phirun Kim[1], *Girdhari Chaudhary*[1], *Yongchae Jeong*[1] ✉
[1]*Division of Electronics and Information Engineering, IT Convergence Research Center, Chonbuk National University, Jollabuk-do, Jeonju, 561-756, Republic of Korea*
✉ *E-mail: ycjeong@jbnu.ac.kr*

Abstract: A wide-stopband attenuation with high-selectivity step impedance resonator (SIR) bandpass filter (BPF) is presented in this study. The T-network stubs are used to produce transmission zeros (TZs) close to the centre frequency (f_0) with a high-selectivity. Moreover, the antiparallel coupled lines can produce a TZ at spurious frequency of conventional SIR BPF for all step impedance ratio (K). For the validation, a half-wavelength ($\lambda/2$) SIR BPF with T-network stubs at the input/output ports was designed at f_0 of 2.6 GHz. From the experiment, the insertion and return losses at f_0 were determined to be 0.91 and 21.25 dB, respectively. The insertion and return losses were better than 1.1 and 16.5 dB, respectively, of the 180 MHz bandwidth. The TZ frequencies (f_{Z1}, f_{Z2}, and f_{Z3}) were located at 1.69 GHz ($0.63f_0$), 2.98 GHz ($1.12f_0$), and 3.17 GHz ($1.19f_0$), respectively, with a high selectivity. The stopband attenuation was better than 25 dB from DC to 2.23 GHz and from 2.89 to 9.82 GHz.

1 Introduction

Wide-stopband attenuation and high-selectivity bandpass filters (BPFs) play an important role in improving the system performance of wireless applications. The transmission zeros (TZs) can improve the passband selectivity of a BPF by using open-/short-circuited stubs transmission lines (TLs) and stepped impedance resonator (SIR) [1–4], shunt-coupled line [5], effective even/odd-mode characteristic impedances and antiparallel coupled line [6–8], and cross-coupling effect [9]. Generally, the passband selectivity of the BPF can be improved by increasing the filter order [10]. However, it may simultaneously increase the circuit size and insertion loss. In [11], the BPF with alternative J/K-inverter quarter-wavelength ($\lambda/4$) resonators was used to improve the passband selectivity with a spurious at 2.9 times of the centre frequency (f_0). However, the passband insertion loss was high. In [12], a high-selectivity microstrip BPF with cascaded-quadruplet $\lambda/4$ resonators was presented, but the first spurious occurred at around $1.8f_0$. In [13, 14], multiple open/short-circuited stubs and inter-digital capacitors were used to improve the stopband performance. Similarly, a modified parallel coupled line with multiple open/short-circuited stubs and shunt parallel coupled lines were proposed for designing BPFs with wide-stopband performance [15, 16]. The multiple TZs in the stopband can be produced by the coupled lines and open/short-circuited stubs. Moreover, a BPF with wide-stopband performance was proposed in [17] by using asymmetric stepped impedance resonators (SIRs). However, a wideband BPF with passband selectivity was introduced using surface acoustic wave (SAW) resonator and microstrip TLs [18]. Although a compact circuit size and passband high selectivity can be obtained using SAW resonators, the wide stopband was limited. Indeed, a high selectivity BPF with eight TZs in the stopband was designed using two ring resonators that coupled each other with $\lambda/4$ coupled length [19]. In [20], a miniaturised, high selective passband, and wide-stopband BPF was designed using multiple open stub-loaded-short-circuited SIR. The TZs and high selective can be obtained by tuning and optimisation process. Similarly, an optimisation hair-pin resonator with input and output cross-coupling was proposed in [21] with high selectivity and wide-stopband performance.

This paper proposes a wide-stopband attenuation and high-selectivity BPF based on $\lambda/2$ SIR and T-network stubs with a low step impedance ratio (K). The T-network stubs can produce a finite-frequency TZs close to the f_0 without much degradation in the passband response. Moreover, the TZ was introduced at the first spurious frequency of the conventional $\lambda/2$ SIR BPF for all K by changing the coupled line to the antiparallel coupled line.

2 Design equations

Fig. 1 shows the stub structures of the short-circuited termination, open-circuited termination, and T-network, respectively. Usually, the open-circuited or short-circuited stubs can be embedded in filters and matching networks only for specific length (i.e. $\lambda/4$ and/or $\lambda/2$ at f_0) to produce TZs at $1.5f_0$, $2f_0$, and $2.5f_0$ [22], and these stub reactances become zero or infinite at f_0. Although the length of the shunt open/short-circuited stubs can vary to load the TZs in the specific frequency, a seriously degrading the passband

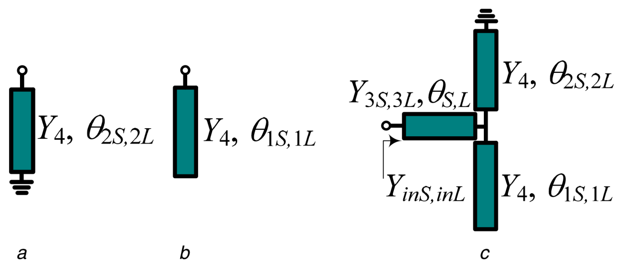

Fig. 1 *Transmission line stubs*
(a) Short-circuited stub, ***(b)*** Open-circuited stub, and ***(c)*** T-network stub

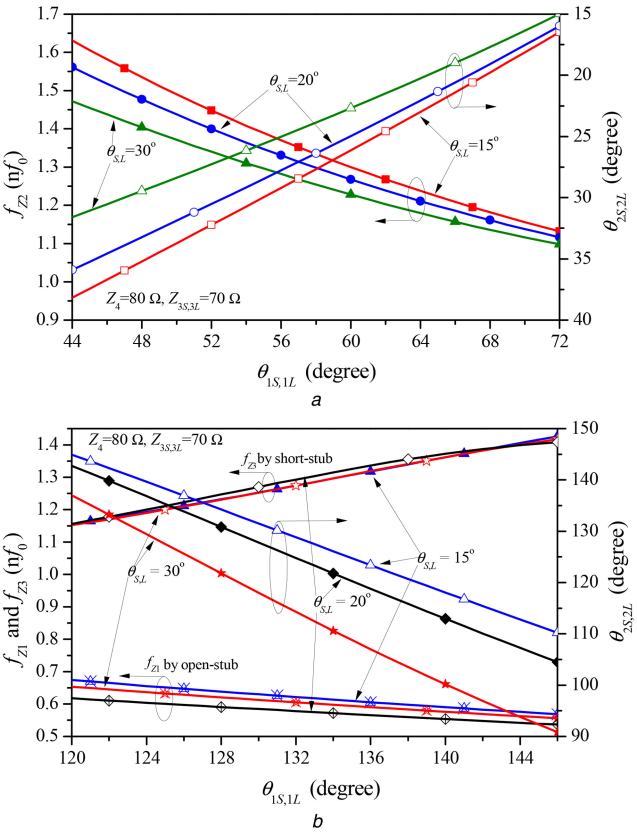

Fig. 2 *Transmission zero and electrical length $\theta_{2S,2L}$ in conditions of*
(a) $\theta_{1S,1L} < \pi/2$ and, ***(b)*** $\theta_{1S,1L} > \pi/2$

response may occur [5] due to the reactance of the stub not being infinite (open circuit) at f_0. Thus, the shunt T-network is proposed simultaneously to produce a finite-frequency TZ and cancel its reactance at the f_0.

Fig. 1*c* shows the T-network stub with electrical parameters of $Y_{3S,3L}$, $\theta_{S,L}$, Y_4, $\theta_{1S,1L}$, and $\theta_{2S,2L}$. The subscripts *S* and *L* stand for the source and load, respectively. The TL with admittance impedance of $Y_{3S,3L}$ is used to extend the connection, and the input admittance of $Y_{inS,inL}$ is found as in (1).

$$Y_{inS,inL} = jY_{3S,3L}\frac{Y_4(\tan\theta_{1S,1L} - \cot\theta_{2S,2L}) + Y_{3S,3L}\tan\theta_{S,L}}{Y_{3S,3L} - Y_4(\tan\theta_{1S,1L} - \cot\theta_{2S,2L})\tan\theta_{S,L}} \quad (1)$$

Where $Y_{3S,3L}$, $\theta_{1S,1L}$, Y_4, and $\theta_{S,L}$, are the predefined variables. Setting (1) equal to zero, the electrical length of $\theta_{2S,2L}$ can be derived as

$$\theta_{2S,2L} = \cot^{-1}(Z_4Y_{3S,3L}\tan\theta_{S,L} + \tan\theta_{1S,1L}) \quad (2)$$

Using (2), the $\theta_{2S,2L}$ of the short-circuited stub can be found by choosing $Y_{3S,3L}$, $\theta_{1S,1L}$, Y_4, and $\theta_{S,L}$ arbitrarily. Then, the input admittance of T-network is cancelled out and become open-circuit at f_0. Moreover, the TZs location can be calculated from (3) by giving $Z_{inS,inL} = 1/Y_{inS,inL} = 0$.

$$Y_{3S,3L} - Y_4(\tan\theta_{1S,1L} - \cot\theta_{2S,2L})\tan\theta_{S,L} = 0 \quad (3)$$

Using (2) and (3), three TZ locations close to f_0 and the electrical length of $\theta_{2S,2L}$ according to the $\theta_{1S,1L}$ can be extracted and plotted in Fig. 2. $\theta_{1S,1L}$ of the open-circuited stub can be varied to produce a finite TZs by fixing $Y_{3S,3L}$ and $\theta_{S,L}$ of the extend lines and Y_4. Then $\theta_{2S,2L}$ of the short-circuited stub can be calculated. Accordingly, the input reactance of the shunt T-network is not affected to the passband (open circuit). For $\theta_{1S,1L} < \pi/2$ as shown in Fig. 2*a*, the TZ is located higher and closer to the f_0 as $\theta_{1S,1L}$ increases. Moreover, $\theta_{2S,2L}$ is decreased as $\theta_{1S,1L}$ increases. In the case of $\theta_{1S,1L} > \pi/2$, the short-circuited stub TL requires a longer length than that in condition of $\theta_{1S,1L} < \pi/2$ for the zero susceptance of $Y_{inS,inL}$. The open-circuited stub TL produces the first TZ lower and closer to the f_0 while the short-circuited stub TL produces the first TZ at higher and closer to the f_0, as can be seem in Fig. 2*b*. The TZs produced by the open-circuited stub and short-circuited stub move towards f_0 as $\theta_{1S,1L}$ decreases. Moreover, the $\theta_{2S,2L}$ increased as $\theta_{1S,1L}$ decreases.

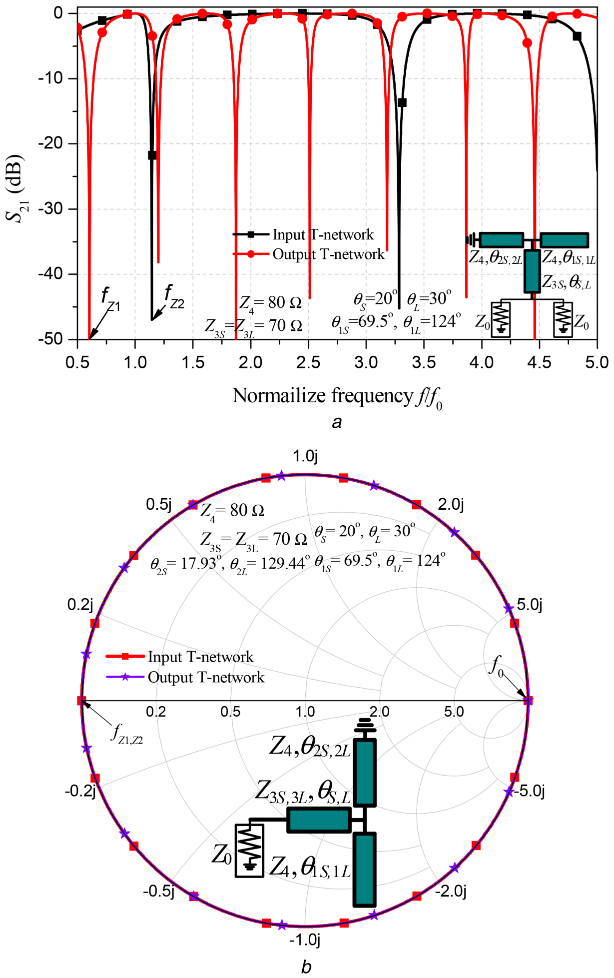

Fig. 3 *Input and output ports T-networks*
(a) S_{21} characteristics and, ***(b)*** Input impedances

Fig. 3*a* shows the S_{21} characteristics of the input/output T-networks stubs. The input/output T-network stub can produce not only two TZs near passband, but also other six TZs in the stopband. The TZs can be located at the desire frequencies by the T-network stubs. The input and output T-networks produce TZs at $1.14f_0$ (f_{Z2}) and $0.6f_0$ (f_{Z1}), respectively. Moreover, Fig. 3*b* shows the input impedance of the input and output T-network stubs on the Smith chart. The input impedances of both T-networks are open (infinite impedance) at the f_0 and short (zero impedance) at the desire TZ frequencies (f_{Z1} and f_{Z2}). Thus, the shunt T-networks do not affect the electrical performance at f_0.

For validation, the T-network stubs are embedded at the input and output ports of the modified $\lambda/2$ SIR BPF. Fig. 4 shows the proposed structure of the SIR BPF consisting of parallel-coupled lines terminated with a shunt T-network stub at the through port and series TL along with antiparallel coupled lines. The filter is composed of *n*-stage resonators with electrical parameters Z_{0ej}, Z_{0oj} ($j = 1, 2, 3, \ldots, n+1$), Z_1, $Z_{3S,3L}$, $\theta_{S,L}$, Z_4, $\theta_{1S,1L}$, $\theta_{2S,2L}$, and θ_0, respectively. θ_0 always has electrical length of $\pi/2$ at the first spurious frequency for all *K* values [10]. Therefore, the antiparallel coupled lines are used to produce a TZ at the first spurious frequency for all *K* values.

The T-network stub and antiparallel coupled line are not effective for the $\lambda/2$ SIR at f_0. Thus, the slope parameter values of all resonators are the same and can be determined as $b = 2\theta_0 Y_2$. Moreover, the J-inverter can be determined from [10]. Then, the even- and odd-mode impedances of the parallel-coupled line at both ends of the proposed BPF can be calculated as (4)

$$Z_{0e(1,n+1)} = Z_2 \frac{1 + J_{1,n+1} Z_2 \csc\theta_0 + J_{1,n+1}^2 Z_2^2}{1 - J_{1,n+1}^2 Z_2^2 \cot^2\theta_0} \quad (4a)$$

$$Z_{0o(1,n+1)} = Z_2 \frac{1 - J_{1,n+1} Z_2 \csc\theta_0 + J_{1,n+1}^2 Z_2^2}{1 - J_{1,n+1}^2 Z_2^2 \cot^2\theta_0} \quad (4b)$$

Moreover, the even- and odd-mode impedances of antiparallel coupled lines can be calculated as (5)

$$Z_{0ei} = Z_2 \frac{1 + J_i^2 Z_2^2 + J_i Z_2 \csc\theta_0 \sec\theta_0}{1 - J_i^2 Z_2^2 \cot^2\theta_0} \quad (5a)$$

$$Z_{0oi} = Z_2 \frac{1 + J_i^2 Z_2^2 - J_i Z_2 \csc\theta_0 \sec\theta_0}{1 - J_i^2 Z_2^2 \cot^2\theta_0} \quad (5b)$$

where $i = 2, 3, \ldots, n$.

Fig. 5 shows the S-parameters of the proposed and conventional SIR BPFs [10] using the lossless TLs and coupled lines with different K. As can be seen in Fig. 5, the passband responses of the BPFs are almost identical. The spurious frequency of conventional BPF with $K = 0.16$ can be moved to high frequency as high as the proposed BPF. However, the characteristic impedance of Z_1 has required up to 310 Ω and it cannot be realised with typical microstrip line. Moreover, the selectivity near to the passband is limited. However, the proposed BPF offers improved selectivity and wide-stopband attenuation with nine TZs using $K = 0.5$. Moreover, the spurious frequency of the proposed BPF can be moved to higher frequency with $K = 0.4$ with an identical TZs as $K = 0.5$. The first spurious frequency is suppressed and shifted to higher with $K = 0.4$. Thus, the proposed SIR BPF with embedded T-network stubs not only can suppress the first spurious frequency with wide-stopband attenuation but also provide high passband selectivity compared to the conventional SIR BPF significantly. According to Fig. 2, the electrical lengths of $\theta_{1S} = 69.5°$ and $\theta_{1L} = 124°$ are selected to produce TZs close to f_0 at $0.6f_0$ and $1.14f_0$, respectively, in conditions of $\theta_S = 20°$ and $\theta_L = 30°$. The specifications and all calculated variables are listed in Table 1.

Since the T-network stubs at the input/output ports have zero susceptance at f_0, the T-network stubs can be symmetrically designed or not in input and output ports without much degradation in the passband performances.

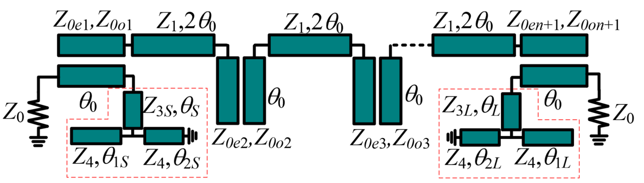

Fig. 4 *Proposed high selectivity bandpass filter*

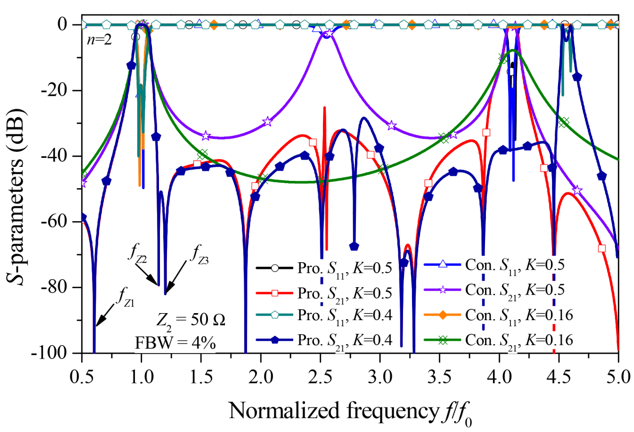

Fig. 5 *S-parameters comparison of the proposed and conventional SIR BPFs with different K*

3 Simulation and measurement results

For the experimental verification, the proposed BPF was designed with the same specifications seen in Section 2 as $K = 0.5$. The layout and photograph of the fabricated high selectivity BPF is shown in Fig. 6. The physical dimensions of the proposed filter are listed in Table 2. Although the T-network stubs of the proposed filter are asymmetrical, the passband performance is maintained, and the filter is implemented in microstrip on a dielectric constant (ε_r) of 2.2 and thickness (h) of 0.787 mm RT/Duroid 5880 substrate. The overall circuit size of the fabricated network is 33 mm × 28 mm ($0.33\lambda_g \times 0.39\lambda_g$). The electromagnetic (EM) simulation was performed using Ansys High-Frequency Structure Simulator (HFSS). The solution frequency of 2.6 GHz, adaption solutions of 20 maximum number, and 0.02 maximum delta S were set in the simulation. Moreover, the driven model solution type and wave ports were used.

Fig. 7 shows the simulation and measurement S-parameters results. The measured S_{21} and S_{11} at $f_0 = 2.6$ GHz were −0.91 dB and −21.25 dB, respectively. The return loss of 16.5 dB was measured from 2.57 to 2.75 GHz (FBW = 7.6%). The measured f_0 was shifted to 2.66 GHz. The antiparallel coupled line had strongly affected the shift of f_0. However, the measured results still agreed well with the results of the simulation. The TZs of f_{Z1}, f_{Z2}, and f_{Z3} were located at 1.69 GHz ($0.63f_0$), 2.98 GHz ($1.12f_0$), and 3.17 GHz ($1.19f_0$), respectively, with a passband high selectivity. The first spurious at 6.67 GHz of the conventional SIR BPF was suppressed to 48.6 dB by a TZ of the antiparallel coupled line. The stopband attenuations of the lower and higher passband were better than 25 dB from DC to 2.23 GHz and from 2.89 to 9.82 GHz ($3.7f_0$), respectively. The first spurious of the proposed filter was measured at 10.2 GHz (3.923 f_0). Thus, it has proved that the proposed SIR BPF can improve passband selectivity and high spurious using T-network and antiparallel coupled lines. The measurement was done in the open space. A performance comparison with state-of-art alternatives is summarised in Table 3. The proposed filter provides a controllable spurious response and finite TZs frequency with a low insertion loss than those of other works.

Table 1 Calculated values of the proposed and conventional SIR BPFs

Ripple = 0.043 dB, FBW = 4%, $n = 2$, $f/f_0 = 1$, $Z_{3S} = Z_{3L} = 70$ Ω, $Z_4 = 80$ Ω, $\theta_S = 20°$, $\theta_L = 30°$ $\theta_{1S} = 69.5°$, $\theta_{1L} = 124°$

	$Z_{0e1,3}/Z_{0o1,3}$ [Ω]	Z_{0e2}/Z_{0o2}	Z_1	K	θ_0	θ_{2S}, nf_0	θ_{2L}	f_{Z1}	f_{Z2}
proposed	90.54/34.96	59.39/42.59	125	0.4	32.31	17.93	129.44	0.6	1.14
	90.61/35.38	59.79/42.24	110	0.5	35.26				
conventional		58.18/43.85							
	113.16/32.92	57.85/44.03	310	0.16	21.88				

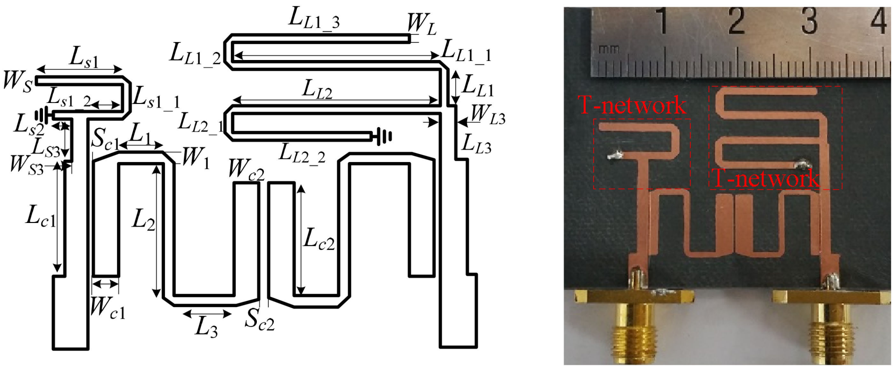

a b

Fig. 6 *Proposed bandpass filter with antiparallel coupled line and shunt T-network stub*
(a) Layout of proposed BPF and, *(b)* Photograph of fabricated proposed BPF

Table 2 Physical dimension of proposed SIR BPFs (unit: mm)

$W_{c1} = 1.25$	$W_{c2} = 0.4$	$W_1 = 0.55$	$L_2 = 8$	$L_1 = L_3 = 3.8$
$S_{c1} = 0.1$	$S_{c2} = 0.4$	$L_{S3} = 4.8$	$L_{L3} = 7$	$W_{S3} = W_{L3} = 1.2$
$L_{c1} = 8.2$	$L_{c2} = 7.9$	$L_{S2} = 3.1$	$L_{S1} = 10$	$W_S = W_L = 0.9$
$L_{S1\_2} = 3.4$	$L_{S1\_1} = 3$	$L_{S2} = 13.7$	$L_{L1\_1} = L_{L1\_2} = 2.5$	
$L_{L2\_2} = 11.2$	$L_{L1} = 2.6$	$L_{L1\_1} = 13$	$L_{L1\_1} = 13.5$	

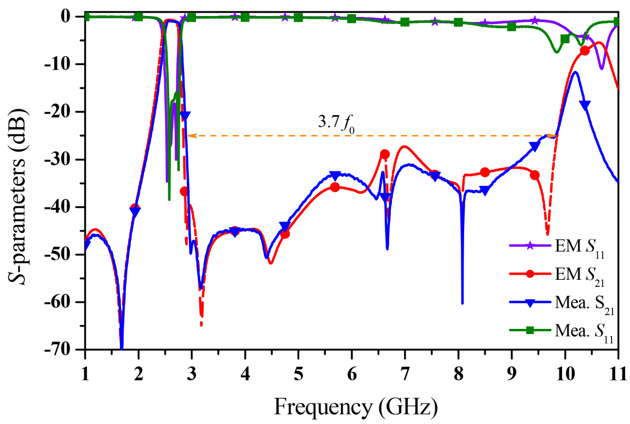

Fig. 7 *EM simulation and measurement results*

Table 3 Performances comparison with previous works

References	f_0, GHz	TZs close to f_0	Spurious	FBW, %	S_{21f0}, dB	Circuit size, $\lambda_0 \times \lambda_0$
[5]	2	$0.84f_0$, $1.175f_0$	NA	≅ 10	1.7	0.79 × 0.06
[6]	2.45	NA	≅ 3.877 f_0	NA	NA	NA
[9] (Fig. 9)	0.955	$0.94f_0$, $1.059f_0$	≅ 2 f_0	7.331	2	0.55 × 0.28
[11] (Fig. 7)	2.4	$0.89f_0$, $1.19f_0$	≅ 3 f_0	NA	2.4	NA
[12]	1.503	$0.92f_0$, $1.084f_0$	≅ 1.73 f_0	10.18	1.28	0.27 × 0.22
[15] (Fig. 14)	1	NA	≅ 14.9 f_0	10	1.93	0.47 × 0.25
[16] (Fig. 9)	0.415	DC, $2.3f_0$	≅ 7.95 f_0	74.7	1.5	NA
[17] (Fig. 6)	1.5	NA	≅ 10.6 f_0	8.9	2.52	0.16 × 0.12
[18] (Fig. 12)	2.02	$0.82f_0$, $1.24f_0$	≅ 1.63 f_0	28.8_{3dB}	1.05	0.24 × 0.45
[19]	2.1	$0.83f_0$, $1.13f_0$	≅ 2.86 f_0	19_{3dB}	1.8	0.39 × 0.28
[20]	0.3405	$0.73f_0$, $1.101f_0$	≅ 4.91 f_0	10	1.2	0.078 × 0.082
this work	2.6	$0.63f_0$, $1.12f_0$	≅ 3.92 f_0	7.6	0.91	0.33 × 0.39

4 Conclusion

A $\lambda/2$ stepped-impedance resonator BPF with antiparallel coupled line and shunt T-network stub is analysed and designed. The capabilities of the antiparallel coupled line and shut T-network stub are extended with the help of producing TZs at the first spurious and in the stopband, respectively, and this provides wide-stopband attenuation and high-selectivity performance. Moreover, the shunt T-network can produce not only a finite-frequency TZ close to f_0, but also cancel the reactance of itself at f_0. The proposed T-network stub is easily used and can be embedded in other kinds of BPF without much degradation in the performance.

5 Acknowledgments

This research was supported by the Basic Science Research Program through the NRF of Korea, funded by Ministry of Education, Science and Technology (2016R1D1A1B03931400).

6 References

[1] Lin, S.-C.: 'Coupled-line filters with stub-embedded resonators using accurate admittance-transformer feeds for flexible termination', *IEEE Trans. Microw. Theory Techn.*, 2014, **62**, (12), pp. 2911–2922

[2] Mandal, M.K., Mondal, P., Sanyal, S.: 'Low insertion loss, wideband bandpass filters with sharp rejection characteristics', *IET Microw. Antennas Propag.*, 2010, **4**, (1), pp. 99–105

[3] Tu, W.-H.: 'Microstrip bandpass filters using cross-sharped triple-mode resonator', *IET Microw. Antennas Propag.*, 2010, **4**, (9), pp. 1421–1426

[4] Wu, S.-R., Hsu, K.-W., Tu, W.-H.: 'Compact wide-stopband microstrip bandpass filter-based on stub-loaded stepped-impedance resonators', *IET Microw. Antennas Propag.*, 2012, **6**, (13), pp. 1422–1428

[5] Chen, C.: 'A coupled-line coupling structure for the design of quasi-elliptic bandpass filters', *IEEE Trans. Microw. Theory Techn.*, 2018, **66**, (4), pp. 1921–1925

[6] Lee, H.-M., Tsai, C.-M.: 'Improved coupled-microstrip filter design using effective even-mode and odd-mode characteristic impedances', *IEEE Trans. Microw. Theory Techn.*, 2005, **53**, (9), pp. 2812–2818

[7] Feng, W., Gao, X., Che, W.: 'Bandpass filters with multiple transmission zeros using open/shorted stubs', *IET Microw. Antennas Propag.*, 2015, **9**, (8), pp. 769–774

[8] Kim, P., Chaudhary, G., Jeong, Y.: 'Impedance matching bandpass filter with a controllable spurious frequency based on $\lambda/2$ stepped impedance resonator', *IET Microw. Antennas Propag.*, 2018, **12**, (12), pp. 1993–2000

[9] Hong, J.-S., Lancaster, M.J.: 'Design of highly selective microstrip bandpass filters with a single pair of attenuation poles at finite frequencies', *IEEE Trans. Microw. Theory Techn.*, 2000, **48**, (7), pp. 1098–1107

[10] Zhu, L., Sun, S., Li, R.: '*Microwave bandpass filters for wideband communications*' (Wiley, New York, 2012), pp. 94–104

[11] Zhang, S., Zhu, L., Weerasekera, R.: 'Synthesis of inline mixed coupled quasi-elliptic bandpass filters based on $\lambda/4$ resonators', *IEEE Trans. Microw. Theory Techn.*, 2015, **63**, (10), pp. 3487–3493

[12] Lin, S.-C.: 'New microstrip cascaded-quadruplet bandpass filter based on connected couplings and short-ended parallel-coupled line', *IEEE Microw. Wirel. Compon. Lett.*, 2014, **24**, (1), pp. 2–4

[13] Tang, C.-W., Hsu, Y.-K.: 'A microstrip bandpass filter with ultra-wide stopband', *IEEE Trans. Microw. Theory Techn.*, 2008, **56**, (6), pp. 1468–1472

[14] Akra, M., Pistono, E., Issa, H., *et al.*: 'Full study of the parallel-coupled stub-loaded resonator: synthesis method in a narrow band with an extended optimal rejection bandwidth', *IEEE Trans. Microw. Theory Techn.*, 2014, **62**, (12), pp. 3380–3392

[15] Chen, F.-C., Hu, H.T., Li, R.-S., *et al.*: 'Design of wide-stopband bandpass filter and diplexer using uniform impedance resonators', *IEEE Trans. Microw. Theory Techn.*, 2016, **64**, (12), pp. 4192–4203

[16] Tang, C.-W., Tseng, C.-T., Chiu, S.-H., *et al.*: 'Design of wide passband/ stopband microstrip bandpass filters with the stepped coupled line', *IEEE Trans. Microw. Theory Techn.*, 2013, **61**, (3), pp. 1095–1103

[17] Kim, C. H., Chang, K.: 'Wide-stopband bandpass filters using asymmetric stepped-impedance resonators', *IEEE Microw. Wirel. Compon. Lett.*, 2013, **23**, (2), pp. 69–71

[18] Lu, X., Mouthaan, K., Yeo, T.S.: 'A wideband bandpass filter with frequency selectivity controlled by SAW resonators', *IEEE Trans. Compon. Packag. Manuf. Technol.*, 2016, **6**, (6), pp. 897–905

[19] Xu, K. D., Zhang, F., Liu, Y., *et al.*: 'Bandpass filter using three pairs of coupled lines with multiple transmission zeros', *IEEE Microw. Wirel. Compon. Lett.*, 2018, **28**, (7), pp. 576–578

[20] Killamsetty, V.K., Mukherjee, B.: 'Compact selective bandpass filter with wide stopband for TETRA band application', *IEEE Trans. Compon. Packag. Manuf. Technol.*, 2018, **8**, (4), pp. 653–659

[21] Bao, M.-J., Wang, X.-G., Cho, Y.-H., *et al.*: 'Design of a four-pole wide stopband bandpass filter using combined quarter-wavelength resonators and stub-loaded SIR'. Proceeding of Asia-Pacific Microw. Conf., Kaohsiung, Taiwan, 2012, pp. 115–117

[22] Kim, P., Chaudhary, G., Jeong, Y.: 'Enhancement impedance transforming ratios of coupled line impedance transformer with wide out-of-band suppression characteristics', *Microw. Optical Technol. Lett.*, 2015, **57**, (7), pp. 1600–1603